frontiers | Frontiers in Earth Science

TYPE Original Research
PUBLISHED 30 July 2025
DOI 10.3389/feart.2025.1618001

OPEN ACCESS

EDITED BY
Wen Nie,
Jiangxi University of Science and Technology, China

REVIEWED BY
Lei Wang,
Ludong University, China
Shuguang Song,
Shandong Jianzhu University, China
Hao Sun,
Ocean University of China, China

*CORRESPONDENCE
Wu Yilin,
yilinw510@163.com

RECEIVED 25 April 2025
ACCEPTED 27 May 2025
PUBLISHED 30 July 2025

CITATION
Jun L, Yilin W, Ya M, Chuanshan W and Wei L (2025) Investigation on the solidification mechanism and mechanical properties of basalt dust waste in soil subgrade construction.
Front. Earth Sci. 13:1618001.
doi: 10.3389/feart.2025.1618001

Investigation on the solidification mechanism and mechanical properties of basalt dust waste in soil subgrade construction

Li Jun[1], Wu Yilin[1,2]*, Ma Ya[1], Wu Chuanshan[2] and Lu Wei[3]

[1]Shandong Hi-speed Construction Management Group Co., Ltd., Jinan, China, [2]Shandong Jide Highway Co., Ltd., Dezhou, China, [3]State Key Laboratory of Tunnel Engineering, Shandong University, Jinan, China

In order to solve the problems of soil scarcity, and the properties of structural loose, poor grading, and poor cohesion of loess in the Huang River area during the construction of the Jibin intercity railway project, to improve the ecological and environmental benefits of the Jibin railway project, and to reduce cement consumption, this article first relies on engineering research to recycle waste stone powder from surrounding stone processing plants, and powder activation and particle size optimization based on self-developed processing system are conducted; Secondly, collect loess soil samples from the Huang River area, conduct soil sample screening and compaction tests, and obtain the particle size distribution and optimal moisture content of the loess; Introducing slag to regulate the activity of stone powder, based on the principle of alkali activation, the orthogonal experimental design method was used to study and compare the influence of alkali activator type, content, and silicon sodium content on the mechanical properties of cementitious materials prepared from basalt rock powder. The variance analysis method was used for parameter sensitivity analysis; Once again, based on the optimal mix ratio determined by the above-mentioned stimulation test and the optimal moisture content and maximum dry density obtained from the compaction test, 7-day unconfined compressive strength tests (20%, 18%, 16%, 14%, 12%, and 10%) were conducted on the silt at different dosages to determine the optimal mixing ratio of the stone powder solidification material. The research results show that the maximum dry density of loess in the Huang River area is 1.84 g/cm^3, and the optimal moisture content is 15.8%; As the proportion of sodium hydroxide and sodium silicate increases, the mechanical strength of the stone powder cured material shows a trend of first decreasing and then increasing, while as the proportion of slag powder decreases, its strength significantly decreases; Micro tests show that with the increase of the amount of stone powder curing materials, a large number of gel materials and ettringite are generated in the improved silt, forming a cementitious space network structure, improving the structural integrity and strength; The on-site test results show that the stone powder improved loess in the yellowing area can meet the requirements of roadbed filling, and the cost is reduced by 51% compared to the cement solidification method. This study provides an economical and environmentally friendly roadbed filling solidification technology for the Jibin high-speed railway and similar projects,

which can provide experimental results and on-site application references for related engineering construction.

KEYWORDS

abandoned stone powder, basalt, yellow floodplain loess, improved soil, roadbed filling material, Jibin railway

Introduction

China is a major producer of stone materials and also faces significant challenges in managing stone processing waste. Long-term accumulation of discarded stone materials not only occupies vast land resources but also causes environmental issues such as dust pollution. Basalt, formed by the rapid cooling of volcanic lava, is dense and highly reactive, making it a critical material for antique-style architecture, European-style buildings, and road construction. However, practical research on the recycling of basalt stone waste remains limited. On the other hand, the Yellow River carries large amounts of silt from the Loess Plateau, which accumulates downstream to form the unique geological environment of the Yellow River floodplain. The floodplain silt exhibits poor gradation, loose structure, and low cohesion, posing significant challenges for engineering applications, particularly in high-speed railway subgrade construction (Wang et al., 2025; Wang et al., 2022; Mi et al., 2021; Bui et al., 2023). The Jinan-Weifang Intercity Railway (Jibin Line), a key component of the Shandong Peninsula urban rail network, is constructed in the Yellow River floodplain area of Jinan, where silt is widely distributed. However, strict restrictions on local quarrying, sand mining, and soil excavation have led to severe shortages of subgrade fill materials. Against the backdrop of growing demand for high-speed rail construction, the limitations of using Yellow River floodplain silt as subgrade filler have become increasingly evident. As noted by scholars such as Weng et al., 2022, its poor engineering properties may lead to subgrade settlement, instability, and other issues, severely impacting railway safety and longevity. Therefore, improving the material properties of Yellow River floodplain silt to meet engineering requirements is of great significance (Zhang et al., 2017; Lu et al., 2023). Traditional cement solidification, while effective in enhancing silt properties, contradicts green development principles due to the high carbon emissions and environmental pollution associated with cement production (An et al., 2013; Zhu et al., 2019; Yao, 2004). In this context, developing a green and efficient method for subgrade filler improvement has become imperative.

Geopolymers, three-dimensional network-structured cementitious materials formed through alkali-activated geopolymerization of aluminosilicate materials, offer excellent mechanical performance, environmental friendliness, high-temperature resistance, and corrosion resistance. In recent years, significant progress has been made in research on geopolymer-based soil improvement using various solid wastes. He et al., 2013 experimentally demonstrated that increasing the Si/Al ratio in fly ash-based geopolymers enhances compressive strength, but excessive ratios inhibit geopolymerization. Similar conclusions were drawn by Silva et al., 2007, who found that variations in the Si/Al ratio within a specific range alter the unconfined compressive strength of geopolymers, providing a theoretical basis for stabilizing problematic soils. Bell, 1994 validated the feasibility of using solidified clay as subgrade filler through CBR tests, compression tests, and unconfined compressive strength tests. Scholars such as Yu and Wang, 1990, Arokiasamy et al., 2025, Tong et al., 2022, Zheng and Zhu, 2013 analyzed reaction mechanisms involving sodium silicate, slag cement, and other activators during hydration, including chemical bond breaking, ion dissolution, and polymerization, offering critical insights into geopolymer reaction mechanisms. Youssef et al., 2019, Hashem et al., 2024, Duan et al., 2015 investigated the effectiveness of slag-fly ash geopolymers, alkali-activated slag geopolymers, and gypsum-activated slag cementitious materials in improving various soil types, confirming the superior performance of geopolymers in soil stabilization. Huang, 2019 used fly ash and cement to solidify red clay, demonstrating significant strength improvements compared to untreated soil. Yang et al., 2022 conducted compaction and California Bearing Ratio (CBR) tests on fly ash-solidified sludge, proving its suitability as road subgrade material. Zheng and Zhu (2013) studied the main reaction products by analyzing the microstructure of alkali activated abrasive blast furnace slag (GGBFS) slurry.

While geopolymers have been extensively studied for enhancing concrete performance and stabilizing soft soils, research on their application in improving Yellow River floodplain silt remains scarce. Key engineering parameters, such as optimal combinations of alkali activators and aluminosilicate materials, are particularly understudied. To address this gap, this study focuses on the Jibin High-Speed Railway project, utilizing basalt waste to prepare geopolymers for improving Yellow River floodplain silt. A series of experiments—including silt property tests, geopolymer material development, geopolymer-silt reinforcement tests, and field trials—were conducted to explore the improvement effects and mechanisms. This research aims to fill the knowledge gap in geopolymer applications for Yellow River floodplain silt, provide a scientific and practical subgrade filler improvement strategy for the Jibin High-Speed Railway and similar projects, and offer a novel pathway for industrial waste recycling, with significant engineering and environmental value.

Study on the properties of loess in the Yellow River floodplain

Soil particle size distribution characteristics

Soil particle gradation is an important soil physical parameter, and a well-graded soil is more likely to achieve the target compaction quality during compaction. Soil particle gradation is an important soil physical parameter, and a well-graded soil is more likely to

FIGURE 1
Sifting test of silt.

TABLE 1 Summary of weights for each particle size.

Grain size (mm)	Weight(g)	Accumulated percentage of soil particles smaller than the particle size
>10	23.86	4.0%
10–5	54.324	9.0%
5–2	98.594	16.4%
2–1	39.76	6.6%
1–0.5	66.4	11.1%
0.5–0.25	55.26	9.2%
0.25–0.0753	123.72	20.6%
<0.0755	138.19	23.0%

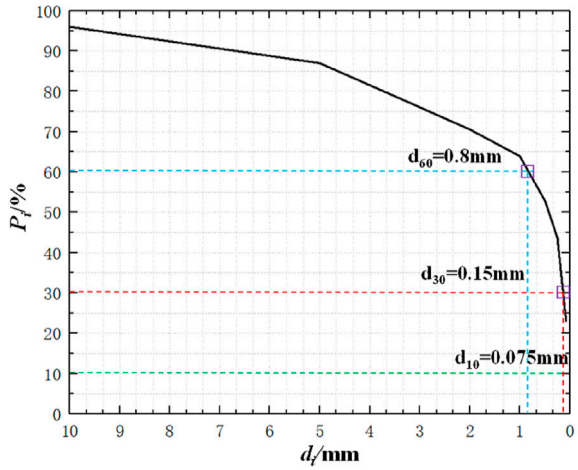

FIGURE 2
Gradation curve of silt particle size.

achieve the target compaction quality during compaction. Therefore, in order to determine whether the soil grading is well obtained, the screening method is used to determine the particle grading of the soil, and the test refers to the "Method of Highway Engineering Soil Test" (Figure 1). The total weight of the soil used in the screening test was 600 g. The obtained test results are shown in Table 1.

The soil particle grading curve obtained from the particle gradation test is shown in Figure 2, and the soil inhomogeneity coefficient index can be obtained from Figure 1: C_u = d60/d10 = 10.7,C_u>5, The silt soil is uneven soil, C_c=(d30·d30)/(d10·d60) = 0.375,1>C_c, The powder soil grading is discontinuous.

Powder earth hit real test

Soil collected on site, determine the moisture content of soil samples in the laboratory, and drying the soil samples after 40 mm sieve, prepare six specimens with different moisture content, moisture content increase of 2%, carry out the compaction test of different moisture content specimens, using Gaussian, Lorentz, log-normal mathematical methods, to determine the optimal moisture content and maximum dry density.

TABLE 2 Specimen compaction results.

Rate of water content (%)	0.13	0.15	0.17	0.18	0.19
Dry density (g/cm^3)	1.75	1.80	1.83	1.68	1.66

Through the compaction test, the maximum dry density of the field silt is 1.84, and the optimal moisture content is 0.158, which lays the foundation for the field test.

The measured water content and the calculated dry density are shown in Table 2, and the solid curve is fitted by polynomial in Figure 3. From Figure 3, the maximum dry density of silt is 1.84 g/cm^3 and the optimal moisture content is 15.8%.

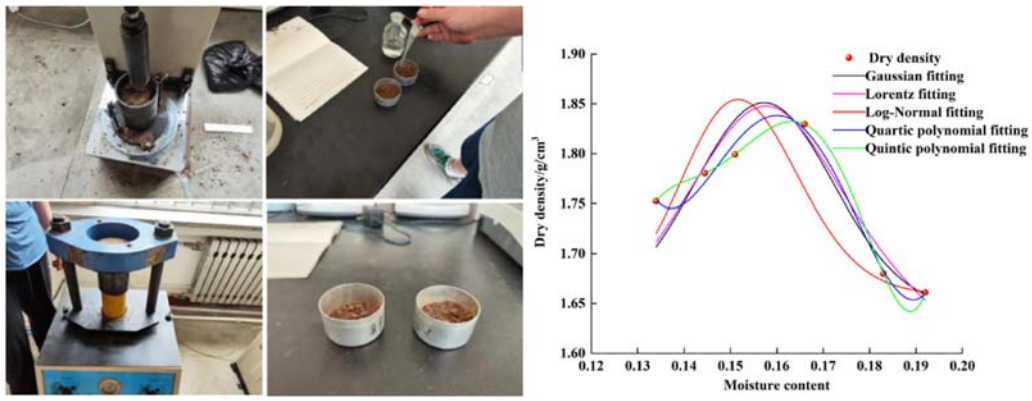

FIGURE 3
Silt performance test.

Waste stone powder curing clay material research and development

This section with stone processing plant collection of basalt waste powder for alkali stimulate solid waste raw materials, the introduction of slag control stone powder activity, the orthogonal test design and sensitivity analysis method, study and compare different alkali excitation agent type, content and silicon sodium content of area powder curing material mechanical properties, get the corresponding mechanism of key parameters.

Activation and particle size optimization of stone powder materials

At present, there are many methods for waste treatment technology, and mechanical crushing is one of the most common technologies. The waste is processed into aggregate or powder of different particle size by crusher and screening equipment. However, if only physical treatment is carried out, the chemical activity of inert solid waste such as stone powder is not fully stimulated, and its reuse performance is low. The heat treatment technology realizes the powder through dehydration, phase change and chemical activation, which can improve its chemical activity. However, high temperature calcination often requires a lot of energy, and improper temperature control may lead to the crystallization or over-burning of the material, but reduce its chemical activity. In addition, the heat treatment technology for complex waste is limited, so it is difficult to achieve refined activity control. Therefore, the author of this paper independently developed the powder activation and particle size optimization system, by accurately controlling the rotary kiln temperature, ball mill powder speed and other parameters, improve the powder activity, reduce energy consumption, optimize the microstructure, and significantly improve the resource utilization efficiency of stone resources in Figure 4.

Test materials and methods

Based on the above stone powder raw materials, in order to further enhance the mechanical properties of powder after excitation, this paper further introduces slag, sodium silicate, lignin and lime powder performance regulation (Figure 5), design shown in Table 3 five factors, each factor design four level, build orthogonal test scheme, at the same time add two groups of comparative test, a total of 16 tests. The specific ratio and the test results are shown in Table 4.

Make the specimens according to the above test scheme, and the sample preparation process is as follows:

(1) Set the mix ratio according to the test scheme and prepare the materials according to the maximum dry density;
(2) Mix Na_2SiO_3 powder and NaOH solid particles with pure water with optimal water content, cool the solution for 2 h to room temperature, and prepare alkali excitation agent;
(3) According to the ratio of materials in the test scheme, call basalt powder, slag, lignin and lime powder, stir evenly in the mixer, add the alkali initiator configured in advance, stir for 5 min;
(4) After full stirring, load the mold and cover the surface with film to keep moisture. After 24 h, remove and maintain in the standard curing room to the test period (temperature is 20°C ± 2°C and humidity is 95% ± 1%). The specific test process is shown in Figure 6.

For parameter sensitivity analysis by analysis of variance, the total variation squared S_T is

$$S_T = \sum_{i=1}^{n} \left(y_i - \frac{Tij}{n} \right)^2 \quad (1)$$

In the formula: Tij represents the sum of experimental results at level i in column j of the orthogonal array, while n denotes the number of trials conducted for the factor.

$$Tij = \sum_{i=1}^{n} y_i \quad (2)$$

$$f = n - 1 \quad (3)$$

$$F = \frac{\frac{s_T}{f}}{s_E} \quad (4)$$

In the formula: f is the degree of freedom; F is the test value in ANOVA and S_E is the mean variance of trial error.

When the F value is used to determine the parameter sensitivity, when $F \geq F0.01$, the factor is the high sensitivity parameter of the

FIGURE 4
Preparation of waste stone powder solidification material.

FIGURE 5
Raw materials for silt solidifying.

TABLE 3 Influencing factor levels.

Horizontal	A	B	C	D	E
	Caustic soda(g)	Mineral adhesive(g)	Mineral waste residue(g)	Lignin(g)	Pulverized lime (g)
1	2.40	2.40	39.75	1.27	3.18
2	4.80	4.80	31.80	2.54	6.36
3	7.20	7.20	23.85	3.82	9.54
4	9.60	9.60	15.90	5.09	12.72

index, which has a highly significant impact on the index. When $F0.01 > F \geq F0.05$, the factor is the sensitivity parameter of the index, significantly affecting the index. When $F0.05 > F \geq F0.1$, the factor is the general sensitivity parameter of the index and has a general significant impact on the index, when $F < F0.1$, the factor is insensitive to the parameter of the index and has no significant impact on the index.

Test results and analysis

The sensitivity analysis of the material parameters

The data analysis was performed using the results presented in Table 4. The significance levels were set based on the actual conditions and were categorized into 0.01, 0.05, and 0.1. Referring to the F-test critical value table, the values are as follows: $F_{0.01}$ (3,5) = 28.237, $F_{0.05}$ (3,5) = 9.013, and $F_{0.1}$ (3,5) = 5.309. The significant results are summarized in Table 5 below.

Using Equations 1–4, based on the variance analysis, it can be concluded that sodium hydroxide and slag powder have a significant impact on the curing material, making them sensitive factors. In contrast, lignin and lime powder do not significantly affect the curing material and are considered insensitive factors. Therefore, the JF-10 group's matching ratio was selected for further experimental trials. A total of three trials were designed, as shown in Table 6.

It can be seen from the test results that the compressive strength of the test piece without lignin and quicklime ratio has increased

10.3389/feart.2025.1618001

TABLE 4 Test protocol.

Group indication	Discard mountain flour (g)	Caustic soda (g)	Mineral adhesive (g)	Mineral waste residue (g)	Lignin (g)	Pulverized lime (g)	Maintain Age (d)	UCS (MPa)
JF-1	31.8	9.6	4.8	39.75	5.09	9.54	7/14	11.63
JF-2	31.8	7.2	4.8	15.9	2.54	3.18	7/14	1.41
JF-3	31.8	2.4	7.2	15.9	5.09	6.36	7/14	2.31
JF-4	31.8	7.2	2.4	31.8	5.09	12.72	7/14	9.59
JF-5	31.8	4.8	4.8	31.8	1.27	6.36	7/14	7.88
JF-6	31.8	2.4	4.8	23.85	3.82	12.72	7/14	7.54
JF-7	31.8	4.8	9.6	23.85	5.09	3.18	7/14	5.61
JF-8	31.8	9.6	9.6	15.9	1.27	12.72	7/14	1.47
JF-9	31.8	9.6	7.2	31.8	3.82	3.18	7/14	7.23
JF-10	31.8	2.4	2.4	39.75	1.27	3.18	7/14	20.85
JF-11	31.8	4.8	7.2	39.75	2.54	12.72	7/14	13.11
JF-12	31.8	9.6	2.4	23.85	2.54	6.36	7/14	4.38
JF-13	31.8	2.4	9.6	31.8	2.54	9.54	7/14	18.46
JF-14	31.8	7.2	7.2	23.85	1.27	9.54	7/14	4.63
JF-15	31.8	4.8	2.4	15.9	3.82	9.54	7/14	2.37
JF-16	31.8	7.2	9.6	39.75	3.82	6.36	7/14	12.48
JF-17	31.8	0	9.6	39.75	3.82	12.72	7/14	15.12
JF-18	31.8	9.60	9.60	15.90	0	12.72	7/14	1.49

FIGURE 6
The test process.

TABLE 5 ANOVA calculations.

Factor	Quadratic sum	Free degree	Mean sum of square	*F*	Conspicuousness	Sensitive characteristics
Caustic soda	182.29	3	60.73	19.704	marked	sensitive
Mineral adhesive	53.433	3	17.814	5.777	generally significant	generally sensitive
Breeze	705.187	3	235.062	76.224	highly significant	high sensitivity
Lignin	24.704	3	8.235	2.67	quiet	insensitivity
Pulverized lime	28.986	3	9.662	3.133	quiet	insensitivity
Deviation	49.342	6	3.084	--	--	--

TABLE 6 Test protocol.

Basalt powder/g	Caustic soda/g	Mineral adhesive/g	Mineral waste residue/g	Lignin/g	Pulverized lime/g	Maintenance period/d	Unconfined compressive strength/MPa
31.8	2.4	2.4	39.75	0	0	7d	31.02
31.8	2.4	2.4	39.75	0	3.18	7d	26.22
31.8	2.4	2.4	39.75	1.27	0	7d	23.90

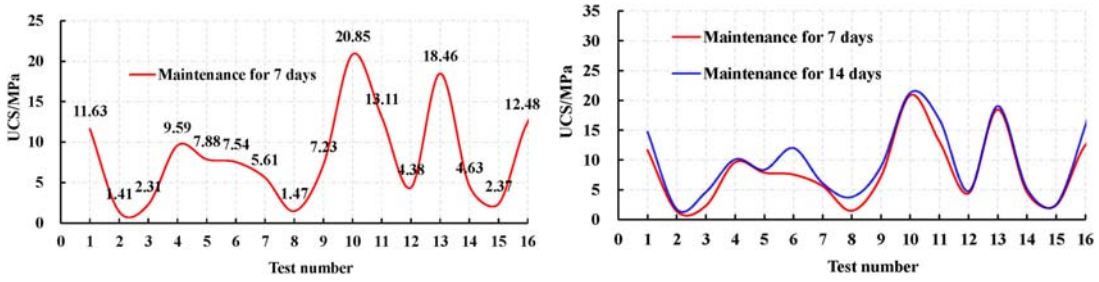

FIGURE 7
Strength curve of geopolymer material.

significantly, which is consistent with the conclusion of variance analysis. Thus, the optimal mix ratio of the curing agent can be determined in Figures 7, 8.

Study on the mechanical strength characteristics of materials under different parameters

Based on the determination of the optimal ratio of curing materials, a series of tests were designed with varying contents of sodium hydroxide, sodium silicate, and slag powder strength. Different ratios of ground polymer specimens were prepared accordingly, as shown in Figure 9 and Table 7. Through mechanical testing of these curing materials, the mechanical properties of the curing materials under different parameter combinations were investigated.

From Figure 10, the following trends can be observed:

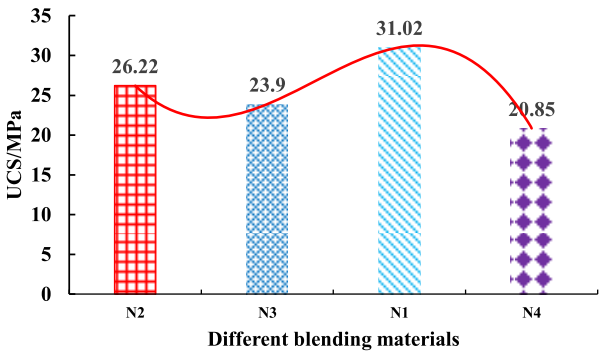

FIGURE 8
Changes in the strength of geopolymer materials after optimization.

FIGURE 9
Specimens before and after the test a.

TABLE 7 Test mechanical scheme of strength of solidifying material with different parameters.

Group indication	Basalt powder(g)	Caustic soda(g)	Mineral adhesive(g)	Breeze (g)	UCS (MPa)
JF1-1	31.8	4.8	2.4	39.75	10.65
JF1-2	31.8	7.2	2.4	39.75	11.88
JF1-3	31.8	9.6	2.4	39.75	17.27
JF2-1	31.8	2.4	4.8	39.75	28.20
JF2-2	31.8	2.4	7.2	39.75	30.71
JF2-3	31.8	2.4	9.6	39.75	35.12
JF3-1	31.8	2.4	2.4	31.8	21.1
JF3-2	31.8	2.4	2.4	23.85	13.56
JF3-3	31.8	2.4	2.4	15.9	6.34
JF4	31.8	2.4	2.4	39.75	31.02

As the content of sodium hydroxide increases, the compressive strength of the curing material initially decreases and then increases. When the content of sodium hydroxide is 4.8 g, the mechanical strength of the curing material first increases and then decreases with the increase in the mixing ratio of sodium silicate. Specifically, when the content of sodium hydroxide is 4.8 g and the content of sodium silicate is 4.8 g, the compressive strength of the curing material reaches its minimum values of 10.65 MPa and 28.2 MPa, respectively. Additionally, as the proportion of slag powder decreases, the mechanical strength of the curing material also exhibits a downward trend.

Study on mechanical properties of waste stone powder

Improved silt strength characteristics

Based on the optimal mix ratio determined through the excitation test and the optimal moisture content and maximum dry density obtained from the compaction test, a 7-day unconfined compressive strength test was conducted at various incorporation ratios (20%, 18%, 16%, 14%, 12%, and 10%) to determine the optimal incorporation ratio of the curing agent material. The specific test protocol is detailed in Table 8 below.

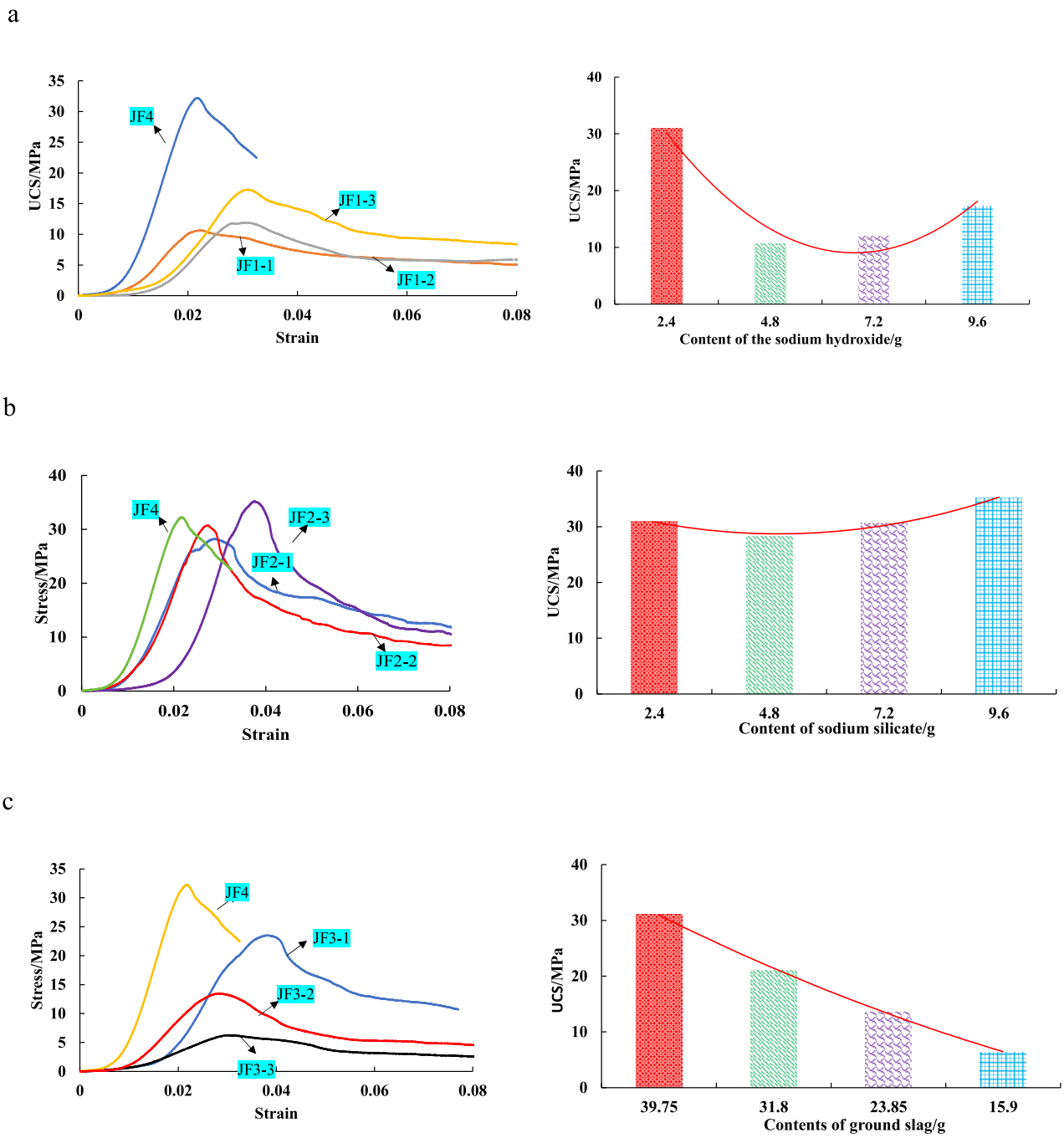

FIGURE 10
Mechanical properties of the solidifying material. **(a)** NaOH content. **(b)** Sodium silicate content. **(c)** Mineral powder content.

Following standard curing for 6 days, the disintegration strength of the samples with 12% and 10% incorporation ratios was found to be 0 MPa, indicating that these samples did not exhibit cohesive strength under disintegration testing conditions in Figure 11.

The unconfined compressive strength (UCS) test results revealed a clear trend: the compressive strength of the cured material increased with higher incorporation ratios of the curing agent. Specifically, the UCS values were 2.74 MPa at a 20% incorporation ratio, 1.66 MPa at 18%, 0.91 MPa at 16%, and 0.45 MPa at 14%. These findings demonstrate that the unconfined compressive strength of the improved soil material is positively correlated with the increase in the incorporation ratio of the curing agent material in Figure 12.

Test of improved microscopic characteristics

Based on the excitation test and the unconfined compressive strength test of the improved soil, representative curing agents with different dosages and excitation ratios were selected for electron

TABLE 8 Test protocol.

Group indication	Soil	Basalt powder	Caustic soda	Mineral adhesive	Ground slag	Water	Maintenance period	Unconfined compressive strength (MPa)
GL-1	144.89	15.21	1.09	1.09	18.84	22.88	7d	2.74
GL-2	148.51	13.69	0.98	0.98	16.95	23.45	7d	1.66
GL-3	152.14	12.17	0.87	0.87	15.07	24.02	7d	0.91
GL-4	155.76	10.65	0.76	0.76	13.19	24.59	7d	0.45
GL-5	159.38	9.13	0.65	0.65	11.30	25.17	7d	0
GL-6	163.00	7.61	0.54	0.54	9.42	25.74	7d	0

FIGURE 11
Geopolymer reinforced silt specimens.

scanning. The microscopic morphology of the samples was observed at different magnifications to analyze the relationship between microstructure and macroscopic mechanical properties. For the excitation test, Groups 2 and 10 were chosen for analysis. The SEM scan results of the samples are shown in Figures 13, 14, with a magnification of 2,500 times.

As observed from the SEM micromorphology of the excitation test specimens, both Groups 2 and 10 exhibited a porous structure. The basalt solid waste particles and slag failed to undergo effective hydration reactions underine alkal excitation, resulting in minimal hydration products. The particles were not well connected, and the overall structure was weak, leading to the low strength of the test specimens. In combination with the ratios and results of all the excitation tests conducted, the primary reason for this phenomenon is the insufficient mixing of slag and the failure of the waste stone powder to hydrate properly, which led to significant granulation within the test structure.

In contrast, the morphology of Group 10 showed that the specimen had good integrity. Under the excitation of sodium hydroxide and sodium silicate, the waste stone powder and slag produced a large amount of hydrated gel materials. These materials filled the pores within the specimen, enhancing structural integrity and significantly improving the strength of the specimen.

As revealed by the SEM microtopography, when the dosage of the curing agent is low, the hydration products are minimal, leading to the formation of large pores within the specimen structure. The structure is predominantly composed of larger soil particles, with poor connectivity between these particles.

With an increasing dosage of the curing agent, the basalt solid waste and slag begin to produce calcium-silicate-hydrate (C-S-H)

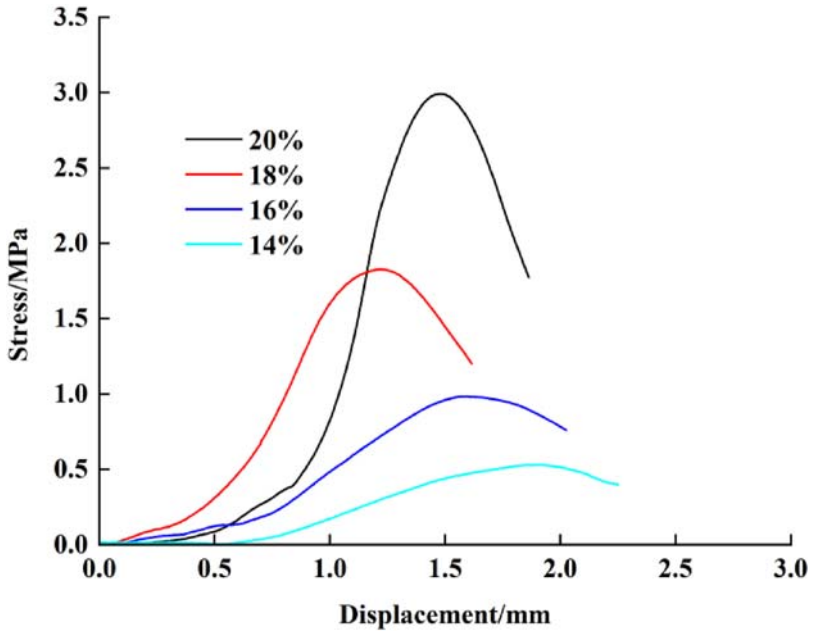

FIGURE 12
Stress curve of solidified soil.

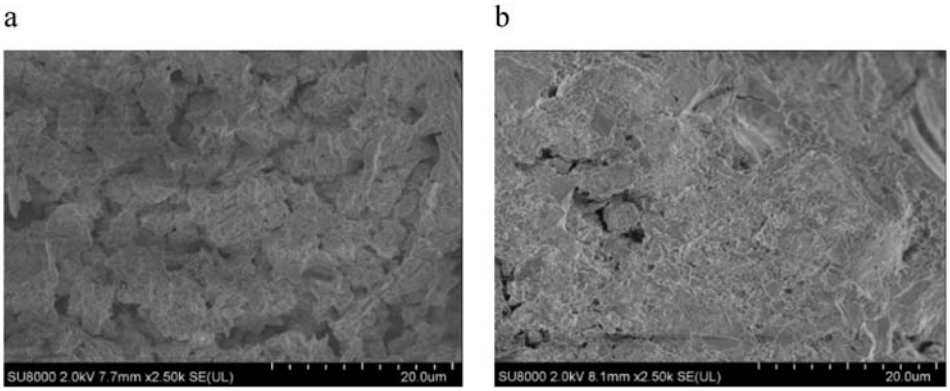

FIGURE 13
SEM images of excitation specimens (×2,500 times). **(a)** Group 2. **(b)** Group 10.

gel materials under the action of alkaline excitation. The C-S-H gel material adheres to the soil particles, forming larger aggregates. Lime (calcium) can effectively fill the gaps between these aggregates. As a result, the soil particles interconnect to form a network structure, enhancing the structural integrity of the improved soil and increasing the system density. This ultimately leads to an increase in the strength of the specimen.

Field test

Testing program

The improvement of the waste stone powder is carried out in three different schemes (Table 9):

(1) First Layer (34 cm Thickness) roll according to the established rolling scheme, test the compaction coefficient K and 7days saturation unlimited compressive strength, if not qualified, continue to roll until the results meet the requirements.
(2) Second Layer (36 cm Thickness): roll according to the established rolling scheme, test the compaction coefficient K and 7days saturation unlimited compressive strength, and continue to roll until the results meet the requirements.
(3) Third Layer (38 cm Thickness): crush according to the established compaction scheme, test the compaction coefficient K and 7days saturation unlimited compressive strength, if not qualified, continue to roll until the results meet the requirements.

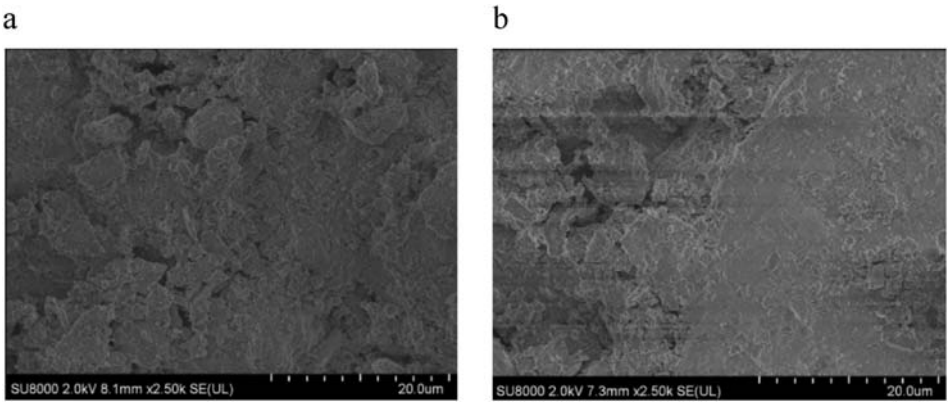

FIGURE 14
Scanning electron microscope images of improved soil specimens (×2,500 times). **(a)** Mixing rate of 20%. **(b)** Mixing rate of 16%.

TABLE 9 Field test protocol.

Plan	Number of filling layers	Paving method	Loose laying depth (cm)	Curing material Content (%)	Roll over the number	Rolling	Speed of travel	Way of rolling
Plan1	First floor	Back method	34	18	Static pressure 1 times + weak vibration 1 times + strong vibration times number (field measured) + weak vibration 1 times + final static pressure 1 time	22t	The rolling speed is controlled within 2 km/h during static pressure and the rolling speed is controlled within 4 km/h during vibration	Back and retreat wrong distance method rolling
Plan2	Second floor		36		Static pressure 1 time + strong vibration times (field measured) + weak vibration 1 time + final static pressure 1 time			
Plan3	Third layer		38		Static pressure 1 times + weak vibration 1 times + strong vibration times number (field measured) + weak vibration 1 times + final static pressure 1 time			

Field test process

Field mixing method for mixing and transportation

The improved silt subgrade material is prepared using mixing equipment at a mixing station, which is equipped with soil crushing devices to eliminate soil clumps larger than 10 mm in diameter. The crushed soil material is then conveyed into a storage bin for the mixer, while the waste stone powder is stored in a separate bin. The moisture content of the raw soil must be adjusted to meet the optimal water content requirements; if necessary, the soil is either dried or mixed with water to achieve the desired moisture level.

FIGURE 15
Paving of geopolymer materials.

FIGURE 16
Subgrade leveling.

Given the mixing station's production capacity, the improved soil mixing station is capable of producing up to 400 cubic meters per hour. Based on the initial setting time of 3 hours, the test section's paving width is set at 4.8 m, with a rolling length of 85 m for the paving operation.

Subgrade substrate treatment

Before the construction, the subgrade surface debris should be removed, and the temporary drainage facilities should be made and kept unblocked. For the local soft areas, the original soil should be replaced and compacted, and then the foundation should be leveled and rolled. The light power touch detector should be tested. The next process can be carried out only after the base test is qualified.

Hierarchical paving

The test section is filled in three layers. Along the longitudinal direction, a set of elevation control points is established every 25 m to monitor the hanging line elevation. White ash is used to mark the edge lines, and the material is discharged in a punctuated manner to control the thickness of each layer during leveling. To ensure the compaction quality of the slope, the subgrade is widened by 50 cm on the outer side during filling. For each layer of filling, compaction is carried out only after confirming that the packing quality, moisture content, soil thickness, and surface flatness meet the actual requirements. Before rolling and tamping, the alcohol combustion method is used to test the moisture content of the subgrade packing. The difference between the packing moisture content and the optimal moisture content should not exceed 2%, and

FIGURE 17
The rolling process of the roller.

FIGURE 18
Compaction degree detection.

the moisture content should not be lower than the optimal value. If the moisture content exceeds the optimal value by more than 2%, the material should be dried first. Only after meeting these requirements should compaction proceed.

Dump trucks transport the packing material, which is then leveled by a bulldozer and grader. The packing material is spread to the specified thicknesses of 34 cm, 36 cm, and 38 cm for each layer in Figure 15. During construction, the edge of the subgrade should be maintained at 50 cm, and the surface of the loose layer should be smooth and uniform. Before paving, a grid is drawn on the subgrade plane using white stone powder to control the feeding quantity and thickness of the loose paving. Based on the grid size, the loading quantity of each vehicle and the number of unloading trucks in each grid are strictly controlled, with material being evenly unloaded in the center of each grid. The grid sizes and material quantities for each layer are as follows: the first layer is 7.5 m × 10 m with 24 m^3 per grid, the second layer is 7 m × 10 m with 24 m^3 per grid, and the third layer is 6.7 m × 10 m with 24 m^3 per grid. A transportation capacity of 24 m^3 per vehicle is sufficient to meet the transportation needs



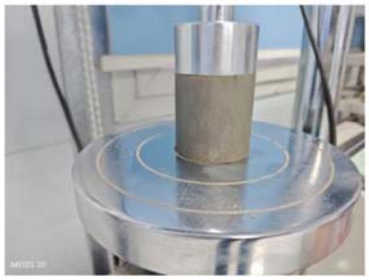
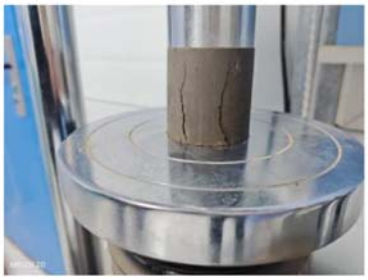

K30=115MPa/m

(Specification requirements:

≥110MPa / m)

Compaction coefficient of

95%

The 7-day unrestrained

intensity was 1.46MPa

FIGURE 19
Field test.

and facilitates unloading control. Paving is carried out from the center to both sides, with a combination of manual and mechanical leveling. The principle of "first low, then high" is followed for uniform paving and layered compaction, and parallel detection is conducted. The following figure illustrates the process of polymer material paving.

The leveling is made according to the field wiring. In the leveling process, the operation is carried out with manual machinery. After the leveling is finished, find out the layout control point and measure the elevation of the top surface of the point. Compared with the ground elevation of the layer, the thickness of the loose paving is strictly controlled. The following figure is the mechanical leveling process in Figure 16.

Roller compaction

Pre-rolling inspection and process optimization

Before rolling, inspect the loose spreading thickness, flatness, and moisture content of the filling layer to ensure they meet the required standards. Utilize various compaction processes to determine the optimal compaction coefficient K and the corresponding equipment combination, compaction times, and compaction speeds. Record the rolling process of the roller to document the most effective parameters for future reference.

A 22T heavy smooth drum vibratory roller is employed for subgrade compaction

The rolling process should proceed from both sides towards the center, moving from lower to higher areas, and using longitudinal advance and retreat rolling techniques. The roller should not turn around during the rolling process to ensure consistent compaction. Additionally, the surface must be kept moist throughout the rolling process to prevent any loosening or peeling of the material in Figure 17.

Rolling methods

(1) First Method (Loose Layer Thickness: 34 cm):

Sequence: Static Pressure → Weak Vibration → Strong Vibration → Weak Vibration → Static Pressure.

Procedure: Begin with static compaction to provide an initial level of density. Follow with weak vibration rolling to further consolidate the material. Then, apply strong vibration rolling, starting from the fourth pass, to achieve maximum compaction. During this phase, conduct synchronous detection of the compaction coefficient and elevation to ensure uniformity. Continue with weak vibration rolling to refine the compaction, and conclude with static pressure to eliminate any wheel tracks and achieve a smooth surface.

(2) Second Method (Loose Layer Thickness: 36 cm):

Sequence: Static Pressure → Strong Vibration → Static Pressure.

Procedure: Initiate with static compaction to establish a base level of density. Proceed directly to strong vibration rolling, starting from the fourth pass, to achieve the required compaction. Conduct synchronous detection of the compaction coefficient and elevation during this phase. Finish with static pressure to eliminate wheel tracks and ensure a smooth, uniform surface.

(3) Third Method (Loose Layer Thickness: 38 cm):

Sequence: Static Pressure → Weak Vibration → Strong Vibration → Weak Vibration → Static Pressure.

Procedure: Start with static compaction to provide an initial level of density. Follow with weak vibration rolling to

begin the compaction process. Then, apply strong vibration rolling, starting from the fourth pass, to achieve maximum compaction. During this phase, conduct synchronous detection of the compaction coefficient and elevation. Continue with weak vibration rolling to refine the compaction, and conclude with static pressure to eliminate any wheel tracks and achieve a smooth surface.

These rolling methods are designed to optimize compaction for different layer thicknesses, ensuring consistent density and surface quality while minimizing the risk of surface defects.

Test results and analysis

Timely quality inspection after compaction. The compaction coefficient K (the ratio of the actual dry density of the subgrade to the maximum dry density of the compaction test sample) and the unlimited compressive strength index are used for control.

The sand filling method is used to test the compaction degree of the subgrade, and the compaction degree of the subgrade is 93.6% to meet the specification requirements (≥92%). The following Figure 18 is the compaction degree detection process.

After on-site sampling, specimen preparation, and conducting the unconfined compressive strength test following 6 days of standard curing and 1 day of water soaking, the unconfined compressive strength of the improved soil reached 1.458 MPa. This value is significantly higher than the design requirements and regulatory standards for chemically modified soil (≥0.25 MPa) in Figure 19.

Conclusion

(1) The silt in the yellow target area exhibits poor gradation characteristics with loose structural configuration and inadequate viscosity, demonstrating a maximum dry density of 1.84 g/cm^3 and an optimum moisture content of 15.8%.

(2) Orthogonal experimental design revealed sodium hydroxide and slag powder as key sensitivity factors influencing the mechanical properties of basalt powder composites. The geopolymer optimal ratio determination demonstrated an inverse correlation between slag powder content and mechanical strength. Notably, the mechanical strength of cured materials exhibited a parabolic response to sodium hydroxide/sodium silicate ratios, characterized by an initial decrease followed by subsequent enhancement with increasing alkaline activator content.

(3) Unconfined compression testing established that 20% curing agent incorporation achieved 7-day strength of 2.74 MPa, with mechanical enhancement showing dosage-dependent characteristics. Microstructural analysis indicated insufficient hydration product formation and weak interparticle connections at low additive levels, accompanied by macroporous structures. Progressive dosage increase promoted gel matrix development and calcium compound precipitation, effectively improving structural integrity through pore-filling effects and enhanced particle bonding.

(4) Three field implementation schemes were systematically executed with strict process control, including critical stages of amended soil mixing, stratified placement (30cm/layer), and intelligent compaction. Quality assurance testing confirmed compliance with engineering specifications, with modified soil achieving ≥95% compaction uniformity and 2.68–2.71 MPa unconfined compressive strength range.

Data availability statement

The original contributions presented in the study are included in the article/supplementary material, further inquiries can be directed to the corresponding author.

Author contributions

LJ: Data curation, Writing – review and editing. WY: Writing – original draft. MY: Data curation, Writing – review and editing. WC: Conceptualization, Writing – review and editing. LW: Software, Writing – original draft.

Funding

The author(s) declare that financial support was received for the research and/or publication of this article. This research was supported in part by the National Natural Science Foundation of China (52309132, 52209140), the Shandong Natural Science Foundation (grant numbers ZR2021ME209, ZR2022QE251), the Higher Education Scientific Research Project 2023 and 2024 (grant numbers 23BR0210, 24SY0104).

Conflict of interest

Authors LJ, WY, and MY were employed by Shandong Hi-speed construction management group Co., Ltd. Authors WY and WC were employed by Shandong Jide Highway Co., Ltd.

The remaining author declares that the research was conducted in the absence of any commercial or financial relationships that could be construed as a potential conflict of interest.

Generative AI statement

The author(s) declare that no Generative AI was used in the creation of this manuscript.

Publisher's note

References

An, P., Zhang, A. J., Liu, H. T., and Wang, T. (2013). Long-term seepage deterioration mechanism and permeability analysis of remodeled saturated loess. *Rock Soil Mech.* 34 (07), 1965–1971.

Arokiasamy, P., Abdullah, M. M. A. B., Arifi, E., Jamil, N. H., Mydin, M. A. O., Rahim, S. Z. A., et al. (2025). Sustainable geopolymer adsorbents utilizing silica fume as a partial replacement for metakaolin in the removal of copper ion from synthesized copper solution. *Case Stud. Constr. Mater.* 22, e04142. doi:10.1016/j.cscm.2024.e04142

Bell, F. G. (1994). An assessment of cement-PFA and lime-PFA used tos tabilize clay-size materials. *Bull. Int. Assoc. Eng. Geol.* 49 (1), 25–32. doi:10.1007/BF02594997

Bui, Q. B., Nguyen, T. P., and Schwede, D. (2023). Manually compressed soil blocks stabilised by fly ash basedgeopolymer: a promising approach for sustainable buildings. *Sci. Rep.* 13, 22905. doi:10.1038/s41598-023-50103-6

Duan, P., Yan, C., Zhou, W., and Luo, W. (2015). Thermal behavior of portland cement and fly ash–metakaolin-based geopolymer cement pastes. *Arabian J. Sci. Eng.* 40 (8), 2261–2269. doi:10.1007/s13369-015-1748-0

Hashem, F. S., Razek, T. A., Mashout, H. A., and Selim, F. A. (2024). Fabrication of slag/ckd one-mix geopolymer cement reinforced by low-cost nano-particles, mechanical behavior and durability performance. *Sci. Rep.* 14 (1), 2549. doi:10.1038/s41598-024-53023-1

He, J., Jie, Y., Zhang, J., Yu, Y., and Zhang, G. (2013). Synthesis and characterization of red mud and rice husk ash-based geopolymer composites. *Cem. and Concr. Compos.* 37, 108–118. doi:10.1016/j.cemconcomp.2012.11.010

Huang, J. (2019). Experimental study on improving red clay road based on fly ash. *Fly. Ash Compr. Util.*, 75–79.

Lu, W., M, L. X., Li, S. C., Xu, Y. D., Wang, L., Zhang, P., et al. (2023). Study on progressive failure behavior and mechanical properties of tunnel arch support structures. *Tunn. Undergr. Sp. Tech.* 140, 105285. doi:10.1016/j.tust.2023.105285

Mi, W. J., Zhang, A. J., Ren, W. Y., Yang, T., Huang, J. S., and Liu, H. T. (2021). Research on the method of reducing the collapsibility of loess by reducing the weight of lightweight soil. *J. Hydraulic Eng.* 52 (01), 51–61.

Silva, P. D., Sagoe-Crenstil, K., and Sirivivatnanon, V. (2007). Kinetics of geopolymerization:role of Al_2O_3 and SiO_2. *Cem. Concr. Res.* 37 (4), 512–518. doi:10.1016/j.cemconres.2007.01.003

Tong, G. Q., Zhang, W. Y., Gao, Y. T., and Tang, X. Y. (2022). Study on mechanical properties and microscopic mechanism of alkali-activated fly ash geopolymers. *Mater. Rep.* 36 (04), 129–134.

Wang, L., Wu, Y., Chen, D. M., Lu, W., Sun, H. B., He, Y. Z., et al. (2025). Study on bearing strength of fiber reinforced polymer anchoring cable in deep roadway. *Sci. Rep15* 4916, 4916. doi:10.1038/s41598-025-85584-0

Wang, R., Hu, Z. P., Wang, L., Bai, L., and Zhao, Z. R. (2022). Dynamic response and long-term settlement of heavy-haul railway embankment in loess area. *J. Railw. Eng.* 39 (01), 7–12.

Weng, X. L., Hu, J. B., Jia, Y., and Zhou, S. Q. (2022). Study on the deformation characteristics of saturation remodeling loess under cyclic traffic loads. *Chin. J. Geotechnical Eng.* 44 (09), 1617–1625.

Yang, Z. J., He, M., Wu, Y., Shi, Y. P., Sun, L., Pan, Z., et al. (2022). Study on mechanical properties and road properties of solidified sludge of slag-fly ash geopolymers. *Bull. Chin. Ceram. Soc.* 41 (02), 693–703.

Yao, W. Z. (2004). Discussion and application of improvement technology of silt clay filler in subgrade of high-speed railway. *Railw. Stand. Des.* 1, 18–22.

Youssef, N., Rabenantoandro, A. Z., Dakhli, Z., Chapiseau, C., Lafhaj, Z., Hage Chehade, F., et al. (2019). Reuse of waste bricks: a new generation of geopolymer bricks. *SN Appl. Sci.* 1 (10), 1252. doi:10.1007/s42452-019-1209-6

Yu, S. R., and Wang, W. M. (1990). Hydration mechanism of clinker-free sodium silicate slag cement. *J. Chin. Ceram. Soc.* 1990 (02), 104–109.

Zhang, Y. C., Yao, Y. G., and Zhou, H. (2017). Experimental study on shear strength and permeability of improved loess in long age. *Rock Soil Mech.* 38 (S2), 170–176.

Zhu, J. F., Rao, C. Y., Tuo, Q. S., Liu, H. X., and Pan, B. J. (2019). Experimental study on reinforcement of silty soil with magnesium sulfide cement composite curing agent. *Chin. J. Rock Mech. Eng.* 38 (S1), 3206–3214.

Zheng, W. Z., and Zhu, J. (2013). The effect of elevated temperature on bond performance of alkali-activated GGBFS paste. *J. Wuhan Univ. Technol.-Mat. Sci. Edit.* 28 (4), 721–725. doi:10.1007/s11595-013-0759-5